http://dx.doi.org/10.35596/1729-7648-2024-22-3-69-75

Original paper

UDC 621.383.525

PERFORMANCE CHARACTERISTICS OF AN INFRARED PHOTODETECTOR USING INTERSUBAND JUNCTIONS IN QUANTUM WELLS BASED ON GALLIUM NITRIDE

VLADISLAV S. VOLCHECK, VIKTOR R. STEMPITSKY

Belarusian State University of Informatics and Radioelectronics (Minsk, Republic of Belarus)

Submitted 22.12.2023

Abstract. A simulation procedure for analyzing the electrical and optical characteristics of an AlGaN/GaN intersubband quantum well middle-wavelength infrared photodetector is presented. The photoconductive gain spectrum was simulated by coupling the drift-diffusion and capture-escape models in the active region of the device structure and by ignoring the contribution of radiative emission. It was shown that the photodetector at zero bias is sensitive over a spectral range from 4 to 6 μm, with the peak absorption occurring at 4.64 μm. The dependence of the available photocurrent on both the wavelength and the angle of incidence of an unpolarized monochromatic beam of light was also evaluated. An assessment of the dark current characteristics was estimated at various temperatures.

Keywords: infrared radiation, quantum well, intersubband transition, simulation, capture-escape model, gallium nitride, optical gain, optoelectronics, absorption, photodetector.

Conflict of interests. The authors declare no conflict of interests.

Gratitude. This work is supported by the grant 1.4.4 of Belarusian National Scientific Research Program "Digital and Space Technologies, Human and Public Safety and National Security".

For citation. Volcheck V. S., Stempitsky V. R. (2024) Performance Characteristics of an Infrared Photodetector Using Intersuband Junctions in Quantum Wells Based on Gallium Nitride. *Doklady BGUIR*. 22 (3), 69–75. http://dx.doi.org/10.35596/1729-7648-2024-22-3-69-75.

ЭКСПЛУАТАЦИОННЫЕ ХАРАКТЕРИСТИКИ ИНФРАКРАСНОГО ФОТОДЕТЕКТОРА, ИСПОЛЬЗУЮЩЕГО МЕЖПОДЗОННЫЕ ПЕРЕХОДЫ В КВАНТОВЫХ ЯМАХ НА ОСНОВЕ НИТРИДА ГАЛЛИЯ

В. С. ВОЛЧЁК, В. Р. СТЕМПИЦКИЙ

Белорусский государственный университет информатики и радиоэлектроники (г. Минск, Республика Беларусь)

Поступила в редакцию 22.12.2023

Аннотация. Представлен метод моделирования электрических и оптических характеристик инфракрасного фотодетектора, использующего межподзонные переходы в квантовых ямах на основе гетероструктуры AlGaN/GaN. Рассчитан спектр коэффициента усиления прибора, полученный в результате численного моделирования в рамках диффузионно-дрейфовой модели и модели захвата-рассасывания носителей с игнорированием вклада радиационной эмиссии. Показано, что диапазон поглощения фотодетектора при нулевом смещении находится в пределах от 4 до 6 мкм, при этом пик поглощения наблюдается

при 4,64 мкм. Произведен расчет зависимости доступного фототока от длины волны и угла падения неполяризованного монохроматического светового луча. Выполнена оценка темного тока при различных температурах.

Ключевые слова: инфракрасное излучение, квантовая яма, межподзонный переход, моделирование, модель захвата-рассасывания, нитрид галлия, оптическое усиление, оптоэлектроника, поглощение, фотодетектор.

Конфликт интересов. Авторы заявляют об отсутствии конфликта интересов.

Благодарность. Работа выполнялась в рамках задания 1.4.4 Государственной программы научных исследований «Цифровые и космические технологии, безопасность человека, общества и государства».

Для цитирования. Волчёк, В. С. Эксплуатационные характеристики инфракрасного фотодетектора, использующего межподзонные переходы в квантовых ямах на основе нитрида галлия / В. С. Волчёк, В. Р. Стемпицкий // Доклады БГУИР. 2024. Т. 22, № 3. С. 69–75. http://dx.doi.org/10.35596/1729-7648-2024-22-3-69-75.

Introduction

The development of infrared optoelectronic devices has been progressing steadily for many decades. Infrared photodetectors are now actively employed in many technologically important applications such as night vision, thermal imaging, environmental sensing and space object detection. Early infrared photodetectors were primarily fabricated from InSb and HgCdTe [1] and utilized intraband transitions. These two materials are suitable for devices operating in the middle-wavelength regime, with wavelengths in a range from 2 to 5 μm. The long-wavelength regime can be accessed only by HgCdTe photodetectors, as their energy levels can be adjusted to absorb electromagnetic radiation in a range from 1 to 30 μm. Although this technology is considered well-established, poor material uniformity and low yield continue to be its major obstacles [2] on account of the naturally weak bond between mercury and tellurium leading to various material instabilities. Moreover, the extreme toxicity of the constituent compounds of HgCdTe photodetectors has recently become of growing concern [3]. These limiting factors provide a strong motivation for exploring novel infrared technologies.

Quantum well infrared photodetectors (QWIPs) based on GaAs are promising optoelectronic devices due to the mature growth and processing technology. These photodetectors have demonstrated consistent results in comparison with HgCdTe devices at low temperatures in the long- and very long-wavelength regimes [4–6]. In later years, GaN technology has also been seen as a potential candidate for developing QWIPs. Due to the large longitudinal optical phonon frequencies, GaN photodetectors are capable to operate at terahertz frequencies that are fundamentally inaccessible to their GaAs-based counterparts [7, 8].

The operation of QWIPs is based on the phenomenon of a quantum particle in a box. The geometry and composition parameters for an alternate array of quantum wells and barriers can be set in such a way that each well contains only one bound state and the sandwich-like device structure forms a superlattice with a quasi-continuum of extended states that carry finite momentum. Electrons from bound states are excited by photons and transferred onto extended states where they generate a photocurrent. The bound-to-extended state transitions are the basic absorption mechanism in QWIP systems and determine both the photoconductive gain spectrum and the quantum efficiency. Among the most appealing features of QWIPs is the possibility to tune the absorption spectrum by adjusting the thickness of quantum wells and the alloy composition of barriers. However, a practical device structure should consist of several tens of wells. This is quite challenging, since the ability to grow epitaxial films over large thicknesses is still limited.

In this work, we present a simulation technique for analyzing the electrical and optical characteristics of an AlGaN/GaN intersubband quantum well middle-wavelength infrared photodetector using a well-known semiconductor device simulator.

Device structure

The two-dimensional AlGaN/GaN QWIP is schematically drawn in Fig. 1. The active region of the device structure is composed of alternate GaN quantum wells and wide band gap $Al_{0.13}Ga_{0.87}N$ barriers. Each well is doped with a donor concentration of $5 \cdot 10^{19}$ cm^{-3}, while each barrier, which should ideally be intrinsic, are realistically doped with a donor concentration of $1 \cdot 10^{10}$ cm^{-3}. The quantum

well thickness is equal to 3 nm, a value determined by reducing the thickness until only one bound state is available. A reasonably large thickness of 0.1 μm is chosen for the barriers to decrease the interaction between the bound states in adjacent quantum wells, thus allowing to regard them as independent of each other. The top and bottom contact regions – emitter and collector, respectively – complete the device structure and are mainly added to bias the active region. The thickness of each contact region is 0.1 μm. The emitter is doped with a donor concentration of $1 \cdot 10^{18}$ cm^{-3}, while a donor concentration of $1 \cdot 10^{19}$ cm^{-3} is introduced to the collector. The width of the device structure is 0.2 μm.

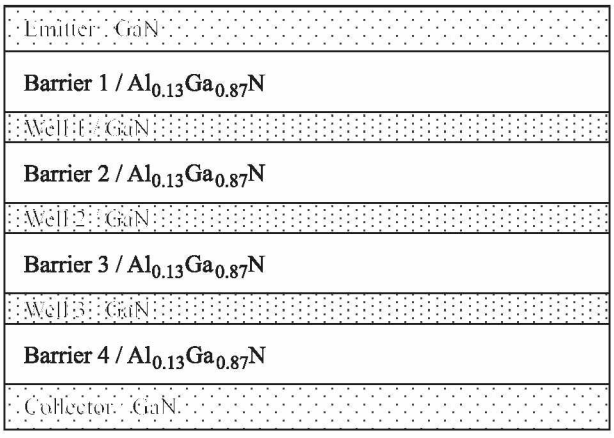

Fig. 1. Device structure

The spatial distribution of both the conduction band edge and the electron quasi-Fermi level of the QWIP at a bias voltage of 0.4 V is shown in Fig 2, *a*. The bound states that play the role of the initial states for electrons in each quantum well are presented in Fig. 2, *b*. The affinity values are set in accordance with the 0.7 rule [9].

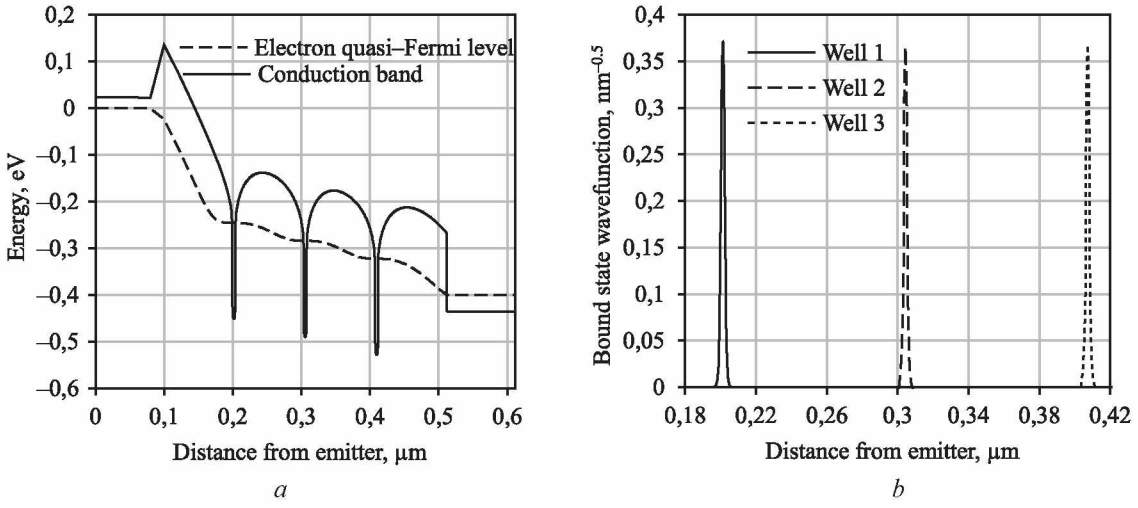

a *b*

Fig. 2. Band diagram: *a* – conduction band edge and electron quasi-Fermi level; *b* – electron bound state wavefunctions

Since electron bound states oscillate with high magnitude, a mesh resolution of at least one tenth of a micrometer is required to accurately depict their wavefunction profiles. Under such strict conditions, simulation time becomes limited by computational capability. For that reason, instead of simulating the full device structure consisting of several tens of quantum wells, we reduced the active region to only three wells. This is utterly reasonable, assuming that the quantum wells do not affect each other to a sufficiently good approximation. As a consequence, the total optical response of the wells can be obtained simply by addition. The scaling down of the active region also leads to the replacement of the quasi-continuum of extended states by a discrete spectrum. Since extended states also oscillate with high magnitude, the convergence of optical transition matrix elements is heavily dependent on the mesh resolution. However, this has an effect only on the magnitude of the spectral response, as the convergence

of its shape is fast at a much larger mesh spacing. Thus, the mesh plays a critical part in the accurate evaluation of both the spectral range of detection and the wavelength of peak detection.

Simulation details

To simulate the optical characteristics of the photodetector, a physical model discretizing the Schrödinger equation along the direction from the emitter to collector is assigned for the quantum wells. A finite difference method is employed to solve this discretized equation.

To calculate the extended states over the active region, a superlattice model is activated. This model also discretizes the Schrödinger equation, but the solutions at each energy must now satisfy the boundary conditions of a plane wave with the same energy penetrating the contact regions.

A three-dimensional semi-classical photocurrent is constituted by the electrons with energy above the barrier band edge. However, some of them are captured by bound states and then escape through phonon emission and absorption, respectively. These two oppositely directed processes are simulated by supplementing the drift-diffusion model with a capture-escape model, which uses the electron capture time as a parameter. With the introduction of this model, the three-dimensional semi-classical and two-dimensional quantum-mechanical bound state densities become more balanced. The ultimate set of Poisson, Schrödinger and drift-diffusion equations is solved until a self-consistent solution is reached.

The device structure is illuminated at room temperature by a black body source placed at a distance of 0.4 μm from the emitter. The energy distribution in terms of the wavelength λ of the electromagnetic radiation emitted by a black body at a given temperature T is fully described by the Planck radiation law. This light is absorbed in each quantum well through bound-to-extended state transitions. To simulate the intersubband absorption of infrared radiation, the electromagnetic field is modelled as a plane wave with a frequency $\omega = 2\pi c/\lambda$, where c is the speed of light. The transverse-magnetic gain coefficient, which gives the quantity of photons with transverse-magnetic polarization produced by intersubband transitions per unit length, is derived using Fermi's golden rule:

$$g = \frac{e^2\pi}{c}\frac{\omega}{n\varepsilon}\sum_{m,n}\left|d_{m,n}\right|^2 \rho \frac{\Gamma/(2\pi)}{\left(E_{mn}-\hbar\omega\right)^2+\left(\Gamma/2\right)^2}\int\left(f_n - f_m\right)dE, \quad (1)$$

where n is the real part of refractive index; ε is the high-frequency permittivity; $d_{m,n}$ is the dipole moment between the initial n and final m intersubband states; ρ is the two-dimensional density of transverse states; Γ is the line width due to Lorentzian broadening; E_{mn} is the difference between energies of the initial E_n and final E_m intersubband states; $\hbar$ is the reduced Planck constant; f_n, f_m are the Fermi-Dirac distribution functions for the initial and final intersubband states integrated over the full transverse energy range E.

The real part of refractive index for GaN is set to 2.38 [10] and is considered independent of the wavelength. The imaginary part is assumed to be zero to exclude the background absorption of light with transverse-electric polarization.

Results and discussion

The transverse-magnetic gain for each quantum well as a function of the wavelength is given in Fig. 3, *a*. Since the gain is the negative of absorption (hence the minus sign in the ordinate axis), it can be seen from the figure that the photodetector is sensitive over a spectral range from 4 to 6 μm. The absorption bandwidth approximately equals to 0.5 μm and the absorption maximum is observed at around 5.2 μm.

At room temperature, the extended states are expected to be almost empty of electrons due to weak thermal excitation, thus resulting in a small dark current. The capture-escape transitions between these states and the bound states are governed by multiple-phonon processes with a time constant of $1 \cdot 10^{-12}$ s. A very small contribution to the dark current is also made by photon emission – the reverse mechanism of photocurrent generation. The spectral resolution of the radiative capture rate is presented in Fig. 3, *b*. The integration of this value with respect to energy gives a time constant of $8 \cdot 10^{-12}$ s. Thus, we can conclude that the radiative intersubband transitions are negligible in QWIPs.

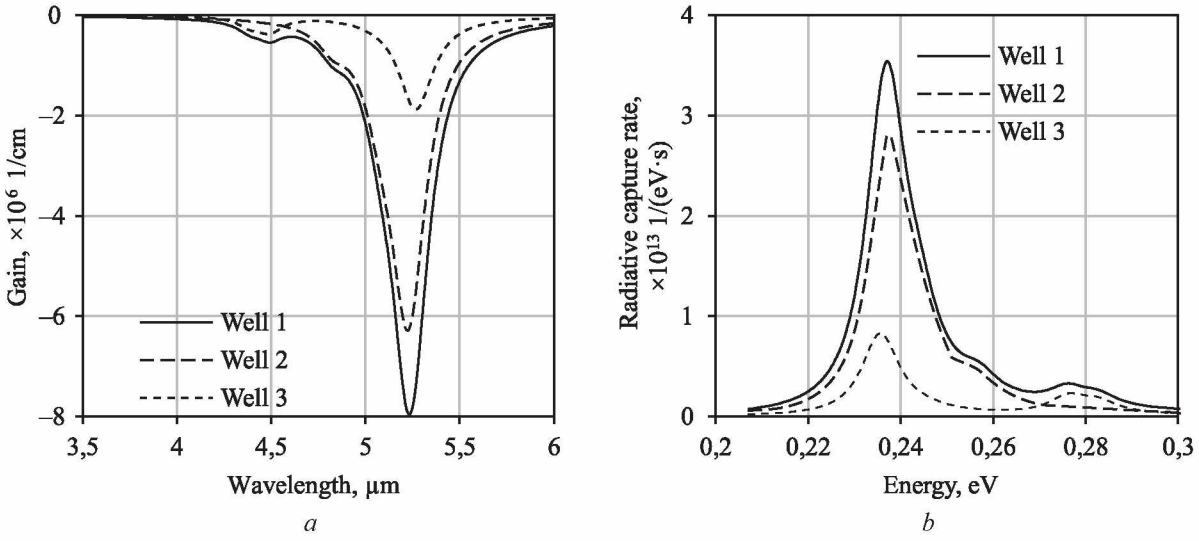

a *b*

Fig. 3. Intersubband transitions: *a* – transverse-magnetic gain vs. wavelength; *b* – radiative capture rate vs. energy

The dark current of the QWIP as a function of the bias voltage at temperatures from 77 to 300 K is shown in Fig. 4. The characteristics are plotted on a logarithmic scale to demonstrate their distinctive form. As seen from the figure, the dark current is estimated at 10^{-18}–10^{-14} A/mm when no voltage is applied and exhibits close to linear variation under all temperature conditions when the voltage is raised. As the temperature grows from 77 to 300 K, the curves go up very rapidly due to intensifying thermal excitation. For example, at a voltage of 0.4 V, the dark current increases from $3.4 \cdot 10^{-15}$ to $5.4 \cdot 10^{-6}$ A/mm.

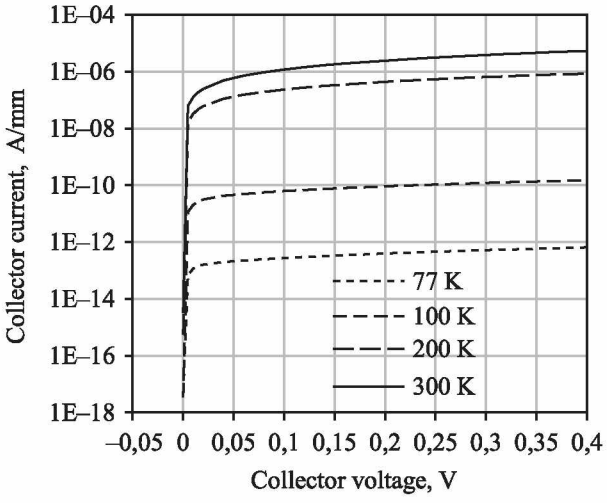

Fig. 4. Dark current at various temperatures

The simulation results obtained when the wavelength of an unpolarized monochromatic beam of light is varied while keeping its angle of incidence constant at 60° with respect to the normal are given in Fig. 5, *a*. The QWIP is zero biased. As expected, the available photocurrent – the hypothetical photocurrent that would be observed if all the electromagnetic radiation absorbed were completely converted into the electric current – has the form equivalent to that of the transverse-magnetic gain, since the only absorption mechanism in the spectral range considered is the intersubband transitions. The maximum available photocurrent of $8.48 \cdot 10^{-7}$ A/mm is observed at 4.64 μm. It should be noted that this maximum point is negatively shifted in the spectrum with respect to the peaks of the gain characteristics because of the applied voltage in the latter case. Since the illuminating black body is closer to the first quantum well, this well generates the bulk of the photocurrent. The available photocurrent as a function of the angle of incidence calculated at a constant wavelength of 4.64 μm is given in Fig. 5, *b*. It is interesting that the maximum of $8.87 \cdot 10^{-7}$ A/mm occurs at 56° and not at right angle, in contrast to what

could be intuitively expected. However, if all the reflections are simulated properly, it may turn out that the beam of light travelling at some acute angle will propagate a shorter path inside the substance before it interacts with the quantum well.

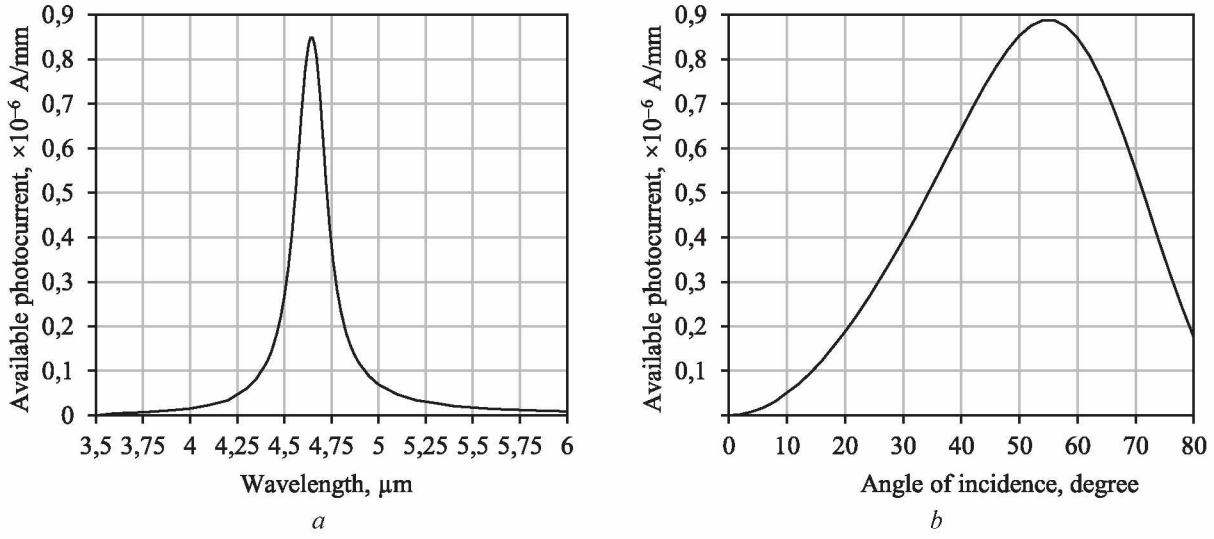

Fig. 5. Spectral and angular response: *a* – available photocurrent vs. wavelength; *b* – available photocurrent vs. angle of incidence

Conclusion

A simulation procedure for analyzing the electrical and optical characteristics of an AlGaN/GaN intersubband QWIP operating in the middle-wavelength regime is presented in the article. The photoconductive gain spectrum was simulated by coupling the drift-diffusion and capture-escape models in the active region and by excluding the contribution of radiative intersubband transitions. The simulation results showed that the photodetector at zero bias is sensitive over a spectral range from 4 to 6 μm, with the maximum absorption being observed at 4.64 μm. The spectral response of the available photocurrent allowed to conclude that the bound-to-extended state transitions are the only absorption mechanism in QWIPs. The angular response of the available photocurrent showed that the maximum absorption can be achieved if the beam of light impinges on the quantum wells at some acute angle.

References

1. Li H., Yang Z. (2023) Recent Progress in Mid-Infrared Photodetection Devices Using 2*D*/*nD* (*n* = 0, 1, 2, 3) Heterostructures. *Materials & Design*. 225. DOI: https://doi.org/10.1016/j.matdes.2022.111446.
2. Rogalski A. (2005) HgCdTe Infrared Detector Material: History, Status and Outlook. *Reports on Progress in Physics*. 68, 2267–2336. DOI: https://doi.org/10.1088/0034-4885/68/10/R01.
3. Rogalski A., Kopytko M., Hu W., Martyniuk P. (2023) Infrared HOT Photodetectors: Status and Outlook. *Sensors*. 23 (17). DOI: https://doi.org/10.3390/s23177564.
4. Levine B. F., Hasnain G., Bethea C. G., Chand N. (1989) Broadband 8–12 μm High-Sensitivity GaAs Quantum Well Infrared Photodetector. *Applied Physics Letters*. 54 (26), 2704–2706. DOI: https://doi.org/10.1063/1.101002.
5. Bethea C. G., Levine B. F., Shen V. O., Abbott R. R., Hseih S. J. (1991) 10-μm GaAs/AlGaAs Multiquantum Well Scanned Array Infrared Imaging Camera. *IEEE Transactions on Electron Devices*. 38 (5), 1118–1123. DOI: https://doi.org/10.1109/16.78387.
6. Patrashin M., Hosako I. (2008) Terahertz Frontside-Illuminated Quantum-Well Photodetector. *Optics Letters*. 33 (2), 168–170. DOI: https://doi.org/10.1364/OL.33.000168.
7. Sudradjat F. F., Zhang W., Woodward J., Durmaz H., Moustakas T. D., Paiella R. (2012) Far-Infrared Intersubband Photodetectors Based on Double-Step III-Nitride Quantum Wells. *Applied Physics Letters*. 100. DOI: https://doi.org/10.1063/1.4729470.
8. Durmaz H., Nothern D., Brummer G., Moustakas T. D., Paiella R. (2016) Terahertz Intersubband Photodetectors Based on Semi-Polar GaN/AlGaN Heterostructures. *Applied Physics Letters*. 108. DOI: https://doi.org/10.1063/1.4950852.

9. Martin G., Botchkarev A., Rockett A., Morkoc H. (1996) Valence-Band Discontinuities of Wurtzite GaN, AlN, and InN Heterojunctions Measured by X-Ray Photoemission Spectroscopy. *Applied Physics Letters*. 68 (18), 2541–2543. DOI: https://doi.org/10.1063/1.116177.
10. Barker A. S., Ilegems M. (1973) Infrared Lattice Vibrations and Free-Electron Dispersion in GaN. *Physical Review B*. 7 (2), 743–750. DOI: https://doi.org/10.1103/PhysRevB.7.743.

Authors' contribution

Volcheck V. S. adapted the physical models, simulated the electrical and optical characteristics of the AlGaN/GaN QWIP, prepared the manuscript of the article.

Stempitsky V. R. formulated the purpose of the work, made corrections in the manuscript.

Information about the authors

Volcheck V. S., Junior Researcher at the Scientific Research Laboratory "Computer-Aided Design of Micro- and Nanoelectronic Systems" (Lab. 4.4) of R&D Department, Belarusian State University of Informatics and Radioelectronics (BSUIR)

Stempitsky V. R., Cand. of Sci., Associate Professor, Vice-Rector for Academic Affairs, Advicer of the Lab. 4.4 of R&D Department, BSUIR

Address for correspondence

220013, Republic of Belarus,
Minsk, P. Brovki St., 6
Belarusian State University
of Informatics and Radioelectronics
Tel.: +375 17 293-84-09
E-mail: vlad.volchek@bsuir.by
Volcheck Vladislav Sergeevich